PAPER

Ambipolar thermoelectric power of chemically-exfoliated RuO_2 nanosheets

To cite this article: Jeongmin Kim *et al* 2018 *Nanotechnology* **29** 015404

View the article online for updates and enhancements.

Ambipolar thermoelectric power of chemically-exfoliated RuO$_2$ nanosheets

Jeongmin Kim[1,4], Somi Yoo[1,4], Hongjae Moon[1], Se Yun Kim[2], Dong-Su Ko[3], Jong Wook Roh[2,5] and Wooyoung Lee[1,5]

[1] Department of Materials Science and Engineering, Yonsei University, 50 Yonsei-ro, Seodaemoon-gu, Seoul, 03722, Republic of Korea
[2] Inorganic Materials Lab, Samsung Advanced Institute of Technology, Samsung Electronics, 130 Samsung-ro, Suwon-si, Gyeonggi-do, 16678, Republic of Korea
[3] Platform Technology Lab, Samsung Advanced Institute of Technology, Samsung Electronics, 130 Samsung-ro, Suwon-si, Gyeonggi-do, 16678, Republic of Korea

E-mail: jw.roh@samsung.com and wooyoung@yonsei.ac.kr

Abstract

The electrical conductivity and Seebeck coefficient of RuO$_2$ nanosheets are enhanced by metal nanoparticle doping using Ag-acetate solutions. In this study, RuO$_2$ monolayer and bilayer nanosheets exfoliated from layered alkali metal ruthenates are transferred to Si substrates for device fabrication, and the temperature dependence of their conductivity and Seebeck coefficients is investigated. For pristine RuO$_2$ nanosheets, the sign of the Seebeck coefficient changes with temperature from 350–450 K. This indicates that the dominant type of charge carrier is dependent on the temperature, and the RuO$_2$ nanosheets show ambipolar carrier transport behavior. By contrast, the sign of the Seebeck coefficient for Ag nanoparticle-doped RuO$_2$ nanosheets does not change with temperature, indicating that the extra charge carriers from metal nanoparticles promote n-type semiconductor behavior.

Supplementary material for this article is available online

(Some figures may appear in colour only in the online journal)

1. Introduction

Since the discovery of graphene [1, 2], two-dimensional materials have attracted much research attention in the fields of optoelectronics and spin-electronics due to their unique properties [3, 4]. Layered structured two-dimensional materials such as transition metal dichalcogenides [5–10], black phosphorous [11–13], and hexagonal boron nitride [14, 15] have unique electrical, optical, mechanical, and thermoelectric properties. Thermoelectrics can convert temperature gradients into electricity and vice versa. Thermoelectric efficiency can be explained using a dimensionless thermoelectric figure of merit $ZT = S^2\sigma T/\kappa$ (Seebeck coefficient S, electrical conductivity σ, absolute temperature T, and thermal conductivity κ). Of the numerous two-dimensional materials, Bi$_2$Te$_3$ and Bi$_2$Se$_3$ nanosheets show high Seebeck coefficients and electrical conductivity [16, 17]. However, there are limitations to their use as thermoelectric generators due to their poor stability. Recently, there has been increased interest in two-dimensional oxide materials showing improved thermal and chemical stability. Two-dimensional ruthenium oxide (RuO$_2$) is particularly noteworthy due to its low resistivity and high thermodynamic stability [18]. Since Dresselhaus first suggested the enhancement of thermoelectric properties with decreasing dimensionality [19, 20], RuO$_2$ nanostructures such as nanorods have seen continued study [21]. However, there are no such studies of RuO$_2$ nanosheets due to the difficulty of exfoliating high-quality nanosheets and measuring their thermoelectric properties.

---

[4] J Kim and S Yoo contributed equally to this work.
[5] Authors to whom any correspondence should be addressed.
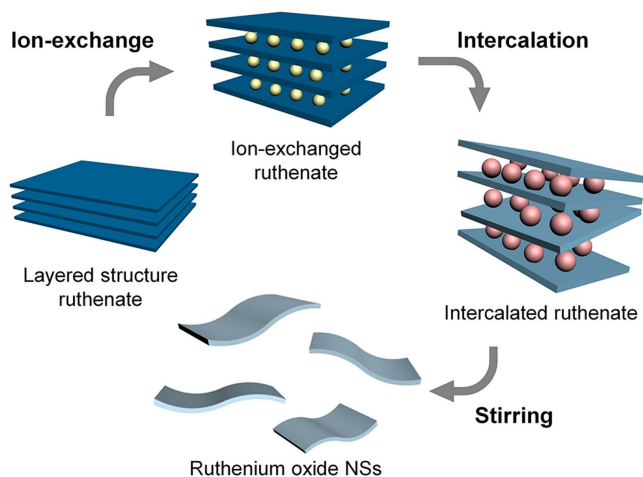
Figure 1. Schematic illustrations of the exfoliation process. The free-standing nanosheets are exfoliated from single-crystalline ruthenium oxide.

In this work, we study the carrier transport properties of RuO_2 nanosheets using thermoelectric property measurements. As the temperature increases above 400 K, the major carrier type of RuO_2 nanosheets is changed, showing ambipolar carrier transport behavior. Moreover, we suggest the use of metal nanoparticle doping to enhance the electrical conductivity and Seebeck coefficient of RuO_2 nanosheets. Metal nanoparticles on the surface of RuO_2 nanosheets can modify the thermoelectric properties of the nanosheets. We conduct the first systematic study on the temperature-dependent thermoelectric properties of individual RuO_2 nanosheets, showing the potential for nanoscale thermoelectrics based on two-dimensional oxide materials.

2. Experimental

2.1. Synthesis of RuO2 nanosheets, device fabrication, and Ag nanoparticle doping

Chemical exfoliation of single crystalline RuO_2 was conducted to prepare RuO_2 nanosheets as shown in figure 1. Layered ruthenates with potassium were formed by annealing RuO_2 (99.9%, Aldrich) and potassium carbonate (K_2CO_3, 99.0%, Aldrich) at 900 °C under N_2 for 24 h using a furnace. In order to form alkali metal ruthenates, the annealed potassium ruthenates were washed with deionized water. These washed alkali metal ruthenates feature gaps between layers, which are beneficial for the exfoliation of nanosheets. The potassium ions in the interlayer were exchanged by immersion in 1 M hydrochloric acid (HCl, 35%, Samchun Chemicals) for 3 days at 60 °C. After acid treatment, protonic-layered ruthenates were immersed into a tetrabutylammonium hydroxide (TBAOH, 99.0 T, Aldrich) solution (40 wt% in H_2O), and TBAOH was intercalated into the interlayers of the ruthenates. The TBAOH solution with layered ruthenates was then stirred for 2 weeks at room temperature. Finally, free-standing RuO_2 nanosheets were synthesized as shown in figure 1.

Figures 2(a) and (b) show the optical microscopy (Olympus) and transmission electron microscopy (TEM, FEI Titan Cubed) images of pristine RuO_2 nanosheets, respectively. The high-resolution TEM image of pristine RuO_2 NS given in figure 2(c) and left inset of figure 2(c) reveals that the nanosheets have a highly ordered honeycomb-like structure. The selected area electron diffraction (SAED) pattern indicates single crystalline RuO_2 nanosheets (right inset of figure 2(c)). The dimensions of the exfoliated RuO_2 nanosheets were measured by scanning electron microscopy (SEM, FEI Nova 450) and atomic force microscopy (AFM, JPK Instruments Nanowizard 1). The lateral size of the nanosheet was at the order of several micrometers, as shown in figure 2(d) and in the inset. The thickness of the RuO_2 nanosheets was in multiples of approximately 1.1 nm and thus, the number of layers of nanosheets was estimated by the height profile analysis, as shown in figure 2(e) [22]. Moreover, the estimated number of layers of the nanosheet was also verified by the electrical conductivity, which was calculated from its measured resistance with respect to its dimensions.

We employed a simple method to decorate metal nanoparticles on the RuO_2 nanosheets to enhance their electrical conductivity and Seebeck coefficient. After immersing pristine RuO_2 nanosheets into 0.05 M Ag-acetate solution for 2 days at room temperature, Ag and AgO_x nanoparticles were formed on the nanosheet surfaces. The nanosheets were washed with deionized water to remove excess nanoparticles. Because the bonding of AgO_x nanoparticles with oxygen atoms on the RuO_2 nanosheets has an adverse effect on the metal doping of the system, the reduction process was carried out by immersing the nanoparticle-decorated RuO_2 nanosheets into 0.05 M $NaBH_4$ for 2 min at room temperature. After this reduction process, only Ag nanoparticles were present on RuO_2 nanosheets. Figure 3 shows the TEM images of the RuO_2 nanosheets decorated with Ag nanoparticles. The Ag nanoparticles were dispersed uniformly on the surface of the RuO_2 nanosheets, as shown in figure 3(b). In order to prove the existence of bonding between the Ag nanoparticles and RuO_2 nanosheets, x-ray photoelectron spectroscopy was employed (see the supplementary data, which is available online at stacks.iop.org/NANO/29/015404/mmedia). It was found that the Ag 3d peak in the spectrum was positioned at 367.5 eV, revealing that the Ag nanoparticles were bonded to the oxygen atoms of RuO_2 nanosheets as Ag_2O [23]. Although it is evident that the Ag nanoparticles were decorated on the surface of RuO_2 nanosheets, the exact doping mechanism in the nanosheets by metal nanoparticles decoration is not fully understood as yet. For determining the doping mechanism and carrier transport properties, thermoelectric devices featuring individual RuO_2 nanosheets were fabricated using photolithography, electron beam lithography, inductively coupled plasma, and Cr/Au metallization. We also measured the electrical conductivity and Seebeck coefficient using a nano-voltmeter (2182A Keithley) and a lock-in amplifier (SR850 Stanford Research Systems).
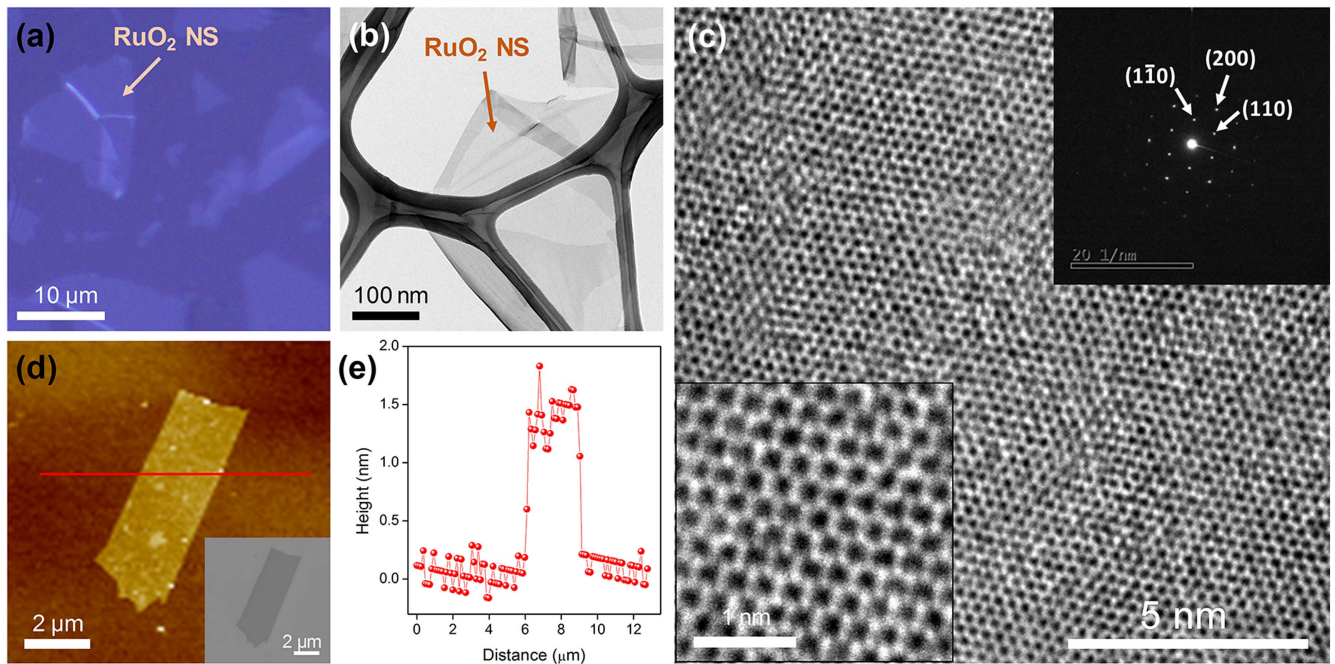
Figure 2. (a) Optical microscopy image of the pristine RuO$_2$ nanosheets on the SiO$_2$/Si substrate. (b) TEM images of the pristine RuO$_2$ nanosheet. (c) High-resolution TEM image of the pristine RuO$_2$ nanosheet. The right inset shows the SAED pattern. (d) AFM images of the pristine RuO$_2$ nanosheet. The inset shows the SEM image. (e) Height profile of the monolayer RuO$_2$ nanosheet.
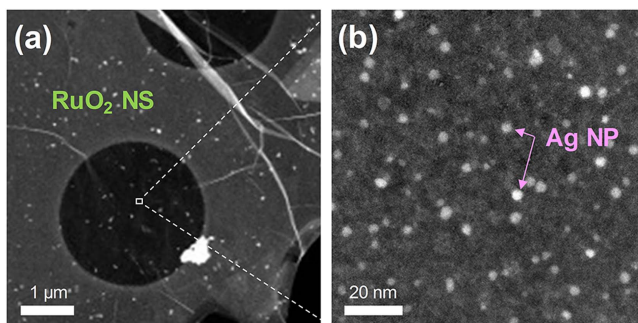
Figure 3. (a) and (b) TEM images of the RuO$_2$ nanosheet decorated with Ag nanoparticles.

2.2. Electrical conductivity and Seebeck coefficient measurements

As shown in figure 4(a), the RuO$_2$ nanosheet thermoelectric devices consisted of a micro-heater, two thermometers, and two resistivity leads [24–26]. Two thermometers and two leads were used for the four-probe measurements, presenting absolute resistance except for contact resistance. The Seebeck coefficient was determined by evaluating the Seebeck voltage and the temperature difference between the two thermometers. Joule heating using the micro-heater created a temperature gradient between the two thermometers. Given the equation for heating power $P = V^2/R$, the Seebeck voltage was proportional to the square of the heater voltage as shown in figure 4(b), indicating a potential difference in the presence of a temperature gradient [27]. The difference in temperature was determined by the temperature coefficient of resistance
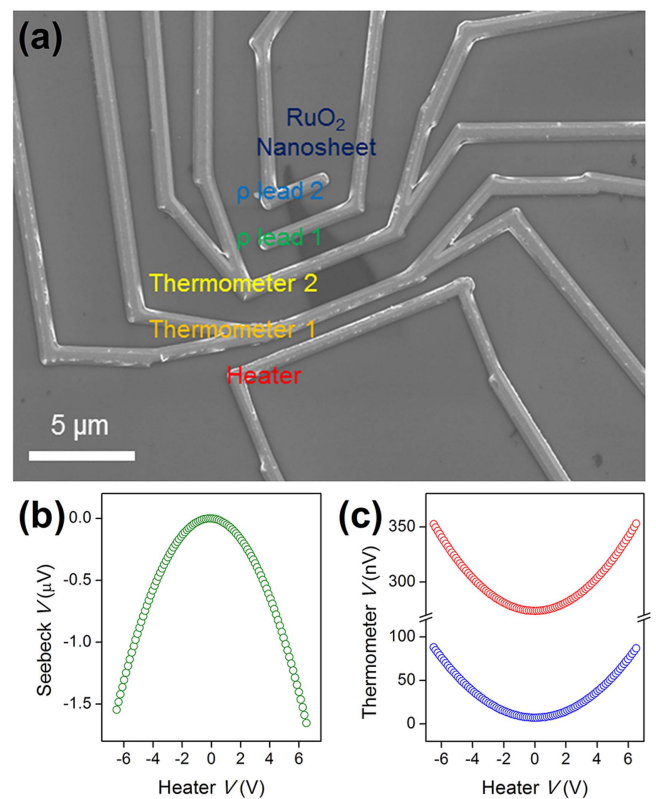
Figure 4. (a) SEM image of an individual RuO$_2$ nanosheet device. (b) Seebeck voltage and (c) thermometer voltages as function of heater voltage.

from the changes in resistance at each thermometer voltage, as shown in figure 4(c). Lastly, the Seebeck coefficient was calculated as $S = \Delta V / \Delta T$ [28–31].
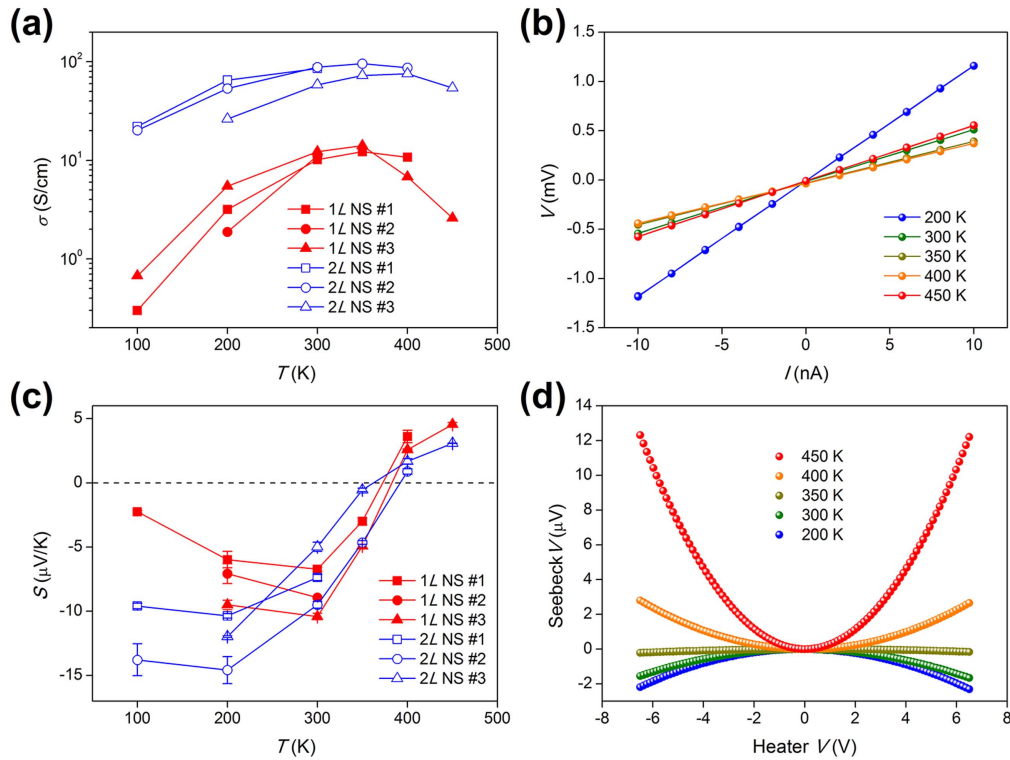
Figure 5. Temperature dependent thermoelectric properties of pristine RuO_2 nanosheets. (a) Electrical conductivity of monolayer and bilayer nanosheets. (b) *I–V* characteristics of bilayer nanosheet #3. (c) Seebeck coefficient of monolayer and bilayer nanosheets. (d) Seebeck voltage of bilayer nanosheet #3.

3. Results and discussion

3.1. Electrical conductivity and Seebeck coefficient of pristine RuO$_2$ nanosheets

Figure 5(a) shows the electrical conductivity of pristine RuO_2 nanosheets as a function of temperature. In the case of bulk RuO_2, temperature-dependent conductivity shows metallic behavior, in that it is determined by the mobility of the charge carrier present; this indicates that carrier-acoustic phonon scattering is the dominant mechanism. On the contrary, the temperature dependence of the RuO_2 nanosheets features semiconducting behavior below 350 K, due to the decreased dimensionality [27, 32, 33]. In the nanostructured crystal, the temperature dependence of the mobility is restricted by the surface scattering due to the low thickness. Thus, the temperature dependent excitation carriers dominate the temperature dependence of conductivity. The circles in figure 5(a) indicate monolayers, while triangles indicate bilayer RuO_2 nanosheets. Although the temperature dependence of the conductivity in both cases is similar, the values of monolayers are lower than that of bilayers, which indicates the surface scattering dominated mobility. The carrier-surface scattering caused by the spatial confinement of nanosheets decreases the mean free path, resulting in a reduction of the mobility of the charge carrier. If the carrier-phonon scattering is dominant, the temperature dependent conductivity exhibits strong metallic behavior. By increasing the temperature up to 350 K,

the RuO_2 nanosheet conductivity increases exponentially, but it decreases at temperatures above 400 K. These results indicate that the temperature dependent carrier-phonon scattering leads to the conductivity decrease at the high temperatures. As shown in figure 5(b), the *I–V* curve of bilayer also reveals temperature dependent conductivity of RuO_2 nanosheets.

The Seebeck coefficient (*S*) is determined by the voltage difference, ΔV, and the temperature difference, ΔT. The voltage difference of an individual nanosheet in this experiment is obtained using Joule heating. If a material has a temperature gradient, it is separated into a hot side and a cold side. Charge carriers move actively at the hot side but are sluggish at the cold side, forming an electric field between the two sides. In the case of n-type materials with electrons as the major carriers, the Seebeck voltage is negative. In contrast, for p-type materials with holes as the major carrier, the Seebeck voltage is positive [34]. Therefore, the sign of the measured Seebeck coefficient can explain the major carrier type in the channel of the material and its dominant charge carrier. Seebeck voltage measurements were conducted at 100–450 K. Using the calibration of the temperature difference at each individual measurement temperature, the Seebeck coefficient can be calculated with the relation $S = \Delta V/\Delta T$. As shown in figure 5(c), the sign of Seebeck coefficients at 100–350 K is negative, while it is positive at 400–450 K. This indicates that the electron charge carriers are dominant at low temperatures and the hole charge
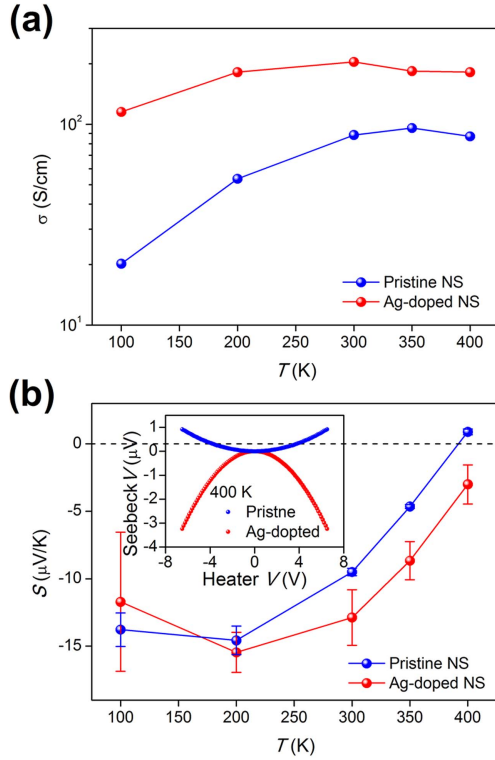
Figure 6. Ag doping effect on temperature dependent thermoelectric properties of a RuO$_2$ nanosheet. (a) Electrical conductivity and (b) Seebeck coefficient of pristine and Ag-doped monolayer nanosheets. Inset shows the Seebeck voltage at 400 K. The blue and red colors indicate pristine and Ag-doped RuO$_2$ nanosheets, respectively.

carriers are dominant at high temperatures. This behavior can be explained by semi-metallic behavior, in that electrons and holes coexist in the RuO$_2$ nanosheets. By increasing the temperature, the holes dominate the charge transport. Although the absolute value of the Seebeck coefficient varies, both monolayer and bilayer nanosheets have a positive Seebeck voltage above 400 K, implying the variation of the dominant charge carrier as shown in figure 5(d).

3.2. Electrical conductivity and Seebeck coefficient of Ag-doped RuO$_2$ nanosheets

The electrical conductivity and Seebeck voltage of metal nanoparticle-doped nanosheets were also measured. As shown in figure 6(a), the electrical conductivity was significantly increased by the Ag nanoparticle doping. The transport properties of semimetals can be explained by two-band system. The total conductivity of RuO$_2$ nanosheets is given by

$$\sigma_{total} = \sigma_h + \sigma_e, \tag{1}$$

where, σ_h and σ_e are the partial electrical conductivity of holes and electrons, respectively. For both pristine and Ag-doped RuO$_2$ monolayer nanosheets, the temperature dependence of the conductivity is similar. However, the

conductivity of the Ag-doped RuO$_2$ nanosheet is much higher than that of the pristine RuO$_2$ nanosheet due to the extra electrons provided by donor carriers. A metal nanoparticle doping effect is demonstrated by these results.

In the two-band system, the Seebeck coefficient of RuO$_2$ nanosheets is given by

$$S_{total} = \frac{\sigma_h S_h + \sigma_e S_e}{\sigma_h + \sigma_e}, \tag{2}$$

where, S_h and S_e are the partial Seebeck coefficient for the holes and electrons, respectively. Therefore, the extra electrons provided by donor carriers increase the contribution of the partial electron Seebeck coefficient to the total Seebeck coefficient, as well as total conductivity. As shown figure 6(b), the temperature dependence of the Seebeck coefficient is similar for both pristine and Ag-doped monolayer nanosheets. The electron charge portion decreases with temperature, while the hole charge portion increases. There is one key difference however, in that the sign of Seebeck coefficient at low temperatures is negative for pristine RuO$_2$ monolayer nanosheets, but is positive at 400 K. The change of sign in Seebeck voltage reveals the variation of major carrier originated by the Ag nanoparticle doping (inset of figure 6(b)). This result indicates that pristine RuO$_2$ nanosheets have semi-metallic properties. By contrast, the sign of the Seebeck coefficient in Ag-doped RuO$_2$ monolayer nanosheets is negative at all temperatures studied here, implying that the doped charge carriers are added by Ag doping effects. This demonstrates that Ag doping of the nanosheet leads to n-type behavior.

3.3. Power factor of pristine and Ag-doped RuO$_2$ nanosheets

Figure 7 shows the power factor of the pristine and Ag-doped RuO$_2$ nanosheets, which was estimated from the measured electrical conductivity and Seebeck coefficient given in figures 5 and 6, respectively. The power factor (σS^2) of a material indicates its electrical thermoelectric performance and is proportional to the square of the Seebeck coefficient. The power factor of the nanosheets was optimized in the temperature range of 200–300 K, where the absolute value of the Seebeck coefficient had increased, as shown in figure 7(a). In this temperature range, the power factor of the bilayer nanosheets was larger than that of the monolayer nanosheets because of the difference in their electrical conductivity. As shown in figure 7(b), the charge carriers introduced by Ag doping increased the power factor in the measured temperature range. This was attributed to the enhancement of the electrical conductivity as a result of the increase in the electron density and the contribution of the electronic partial Seebeck coefficient in the two-band system.

4. Conclusions

We investigated the thermoelectric properties of monolayer and bilayer RuO$_2$ nanosheets, and compared pristine and
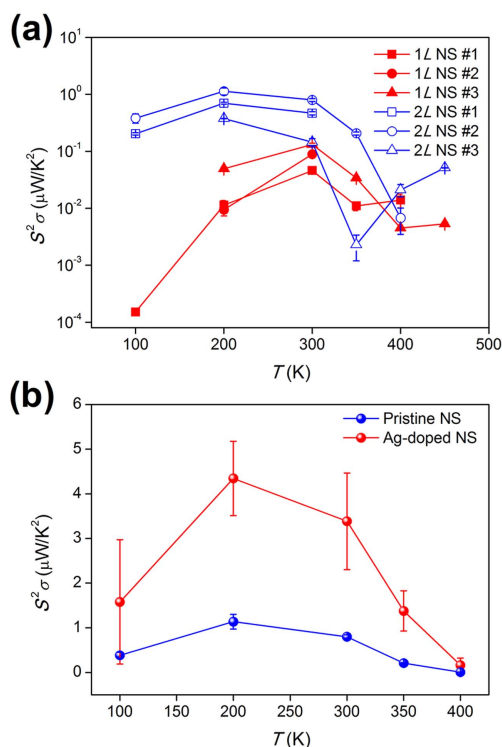
Figure 7. Estimation of the power factors of the RuO_2 nanosheets. Temperature-dependent power factor of the (a) monolayer and bilayer nanosheets and (b) pristine and Ag-doped nanosheets.

Ag-doped RuO_2 nanosheets in terms of their thermoelectric properties. The electrical conductivity and the absolute value of the Seebeck coefficient of the RuO_2 nanosheets were enhanced by doping them with Ag metal nanoparticles using Ag acetate solution. Two key findings came out of our thermoelectric property analysis, those being the ambipolar carrier transport properties of RuO_2 nanosheets and the n-type semiconducting behavior of Ag nanoparticle-doped RuO_2 nanosheets. These results show the potential of RuO_2 nanosheets for use in nanostructured thermoelectric materials.

Acknowledgments

ORCID iDs

Wooyoung Lee ⓘ https://orcid.org/0000-0001-8406-4324

References

[1] Novoselov K S, Geim A K, Morozov S V, Jiang D, Katsnelson M I, Grigorieva I V, Dubonos S V and Firsov A A 2005 *Nature* **438** 197
[2] Geim A K and Novoselov K S 2007 *Nat. Mater.* **6** 183
[3] Bonaccorso F, Sun Z, Hasan T and Ferrari A C 2010 *Nat. Photon.* **4** 611
[4] Han W, Kawakami R K, Gmitra M and Fabian J 2014 *Nat. Nano* **9** 794
[5] Radisavljevic B, Radenovic A, Brivio J, Giacometti V and Kis A 2011 *Nat. Nano* **6** 147
[6] Zhang Y *et al* 2014 *Nat. Nano* **9** 111
[7] Voiry D *et al* 2013 *Nat. Mater.* **12** 850
[8] Pletikosić I, Ali M N, Fedorov A V, Cava R J and Valla T 2014 *Phys. Rev. Lett.* **113** 216601
[9] Wang Q H, Kalantar-Zadeh K, Kis A, Coleman J N and Strano M S 2012 *Nat. Nano* **7** 699
[10] Wickramaratne D, Zahid F and Lake R K 2014 *J. Chem. Phys.* **140** 124710
[11] Li L, Yu Y, Ye G J, Ge Q, Ou X, Wu H, Feng D, Chen X H and Zhang Y 2014 *Nat. Nano* **9** 372
[12] Xia F, Wang H and Jia Y 2014 *Nat. Commun.* **5** 4458
[13] Fei R, Faghaninia A, Soklaski R, Yan J-A, Lo C and Yang L 2014 *Nano Lett.* **14** 6393
[14] Watanabe K, Taniguchi T and Kanda H 2004 *Nat. Mater.* **3** 404
[15] Song L *et al* 2010 *Nano Lett.* **10** 3209
[16] Hong M, Chasapis T C, Chen Z-G, Yang L, Kanatzidis M G, Snyder G J and Zou J 2016 *ACS Nano* **10** 4719
[17] Hong M, Chen Z-G, Yang L, Han G and Zou J 2015 *Adv. Electron. Mater.* **1** 1500025
[18] Ohta H, Sugiura K and Koumoto K 2008 *Inorg. Chem.* **47** 8429
[19] Hicks L D and Dresselhaus M S 1993 *Phys. Rev.* B **47** 12727
[20] Hicks L D and Dresselhaus M S 1993 *Phys. Rev.* B **47** 16631
[21] Music D, Basse F H-U, Haßdorf R and Schneider J M 2010 *J. Appl. Phys.* **108** 013707
[22] Sato J, Kato H, Kimura M, Fukuda K and Sugimoto W 2010 *Langmuir* **26** 18049
[23] Morales J, Sánchez L, Martín F, Ramos-Barrado J R and Sánchez M 2004 *J. Electrochem. Soc.* **151** A151
[24] Shim W, Ham J, Kim J and Lee W 2009 *Appl. Phys. Lett.* **95** 232107
[25] Kim J, Lee S, Brovman Y M, Kim M, Kim P and Lee W 2014 *Appl. Phys. Lett.* **104** 043105
[26] Kim J, Kim D, Chang T and Lee W 2014 *Appl. Phys. Lett.* **105** 123107
[27] Kim J, Lee S, Brovman Y M, Kim P and Lee W 2015 *Nanoscale* **7** 5053
[28] Lee C-H, Yi G-C, Zuev Y M and Kim P 2009 *Appl. Phys. Lett.* **94** 022106
[29] Shim W, Ham J, Lee K-I, Jeung W Y, Johnson M and Lee W 2009 *Nano Lett.* **9** 18
[30] Zuev Y M, Chang W and Kim P 2009 *Phys. Rev. Lett.* **102** 096807
[31] Zuev Y M, Lee J S, Galloy C, Park H and Kim P 2010 *Nano Lett.* **10** 3037
[32] Zhang Z, Sun X, Dresselhaus M S, Ying J Y and Heremans J 2000 *Phys. Rev.* B **61** 4850
[33] Heremans J, Thrush C M, Lin Y-M, Cronin S, Zhang Z, Dresselhaus M S and Mansfield J F 2000 *Phys. Rev.* B **61** 2921
[34] Pal K, Anand S and Waghmare U V 2015 *J. Mater. Chem.* C **3** 12130